

**Relativistic modified Bessel-Gaussian beam generated from plasma-based beam braiding**

Bifeng Lei <sup>1,2,3,\*</sup>, Daniel Seipt <sup>1,2,3</sup>, Mingyuan Shi,<sup>1,2,3</sup> Bin Liu,<sup>1,2,†</sup> Jingwei Wang,<sup>4</sup>  
Matt Zepf,<sup>1,2,3</sup> and Sergey G. Rykovanov<sup>5,‡</sup>


<sup>1</sup>Helmholtz Institute Jena, Fröbelstieg 3, 07743 Jena, Germany

<sup>2</sup>GSI Helmholtzzentrum für Schwerionenforschung GmbH, Planckstrasse 1, 64291 Darmstadt, Germany

<sup>3</sup>Faculty of Physics and Astronomy, Friedrich-Schiller-Universität Jena, 07743 Jena, Germany

<sup>4</sup>Shanghai Institute of Optics and Fine Mechanics, Chinese Academy of Sciences, 201800 Shanghai, China

<sup>5</sup>Center for Computational and Data-Intensive Science and Engineering, Skolkovo Institute of Science and Technology, Moscow 121205, Russia

 (Received 27 January 2021; revised 21 May 2021; accepted 10 August 2021; published 20 August 2021)

We theoretically and numerically demonstrate the generation of a relativistic modified Bessel-Gaussian beam (MBGB) via plasma-based beam braiding. It is realized by injecting several intense Gaussian pulses with well-designed offsets and angles into an underdense plasma channel which acts as a laser-pulse combiner via refractive coupling. The MBGB propagates stably in the plasma channel with a well-controlled orbital angular momentum of large value, exciting a twisted plasma wave. After leaving the plasma, it becomes unguided and survives in vacuum for at least hundreds of femtoseconds. This method is insensitive to the initial laser injection conditions and thus should be robust for experimental implementation. It provides an alternative approach in generating high-quality tunable intense optical vortex beams which are desired for various applications.

DOI: [10.1103/PhysRevA.104.L021501](https://doi.org/10.1103/PhysRevA.104.L021501)

Over the last decades considerable progress has been seen in the development of optical vortex beams (OVBs). An OVB carries orbital angular momentum (OAM) and can subtly connect macroscopic to microscopic optics [1]. It fundamentally provides a new optical degree of freedom in the understanding of a wide range of optical and physical phenomena, especially in the way of OAM manipulation. Recently, much attention has been paid to intense or ultraintense OVBs [2] which transfer the OAM from photons to plasma particles, exciting helical plasma waves and resulting in innovative applications such as fundamental research [3–6], strong vortex field-plasma interactions for quantum photonics [7], particle acceleration [8–10], extreme magnetic field generation [11,12], the creation of electron vortices [13], polarized electron beam production [14], radiation generation [15,16], and optical controlling of the plasma wakefield [17].

So far, much effort has been made in generating ultraintense OVBs. Recently proposed methods based on classical optical materials can significantly increase the intensity [18–20] or stability [21] of OVBs. Plasma-based approaches promise ultrahigh intensity as there is no damage threshold in the plasma medium. Most of them are focusing on the generation of paraxial Laguerre-Gaussian beams (LGBs) by using a phase mirror [22] or an equivalent, e.g., transient plasma holograms [23], Raman amplification [24], and a light fan [25]. With these methods, an ultraintense OVB can be

generated, focused via an off-axis parabola in vacuum, and then injected into a plasma to achieve different applications. However, it turned out to be a big challenge to generate a perfect ultraintense OVB [26–28]. It seems that for an OVB which has a distinct helical wave front, a small intensity fluctuation or phase aberration can result in a significant imperfection on the focused beam.

In this Letter, we propose a different approach in which a relativistic OVB is generated in a plasma by using focused Gaussian pulses. It promises high beam quality and is suitable for *in situ* applications in the plasma. The OVB is formed via a plasma-based beam braiding (PBB) method. The method employs underdense microscale parabolic plasma channels which have been widely used in plasma wakefield acceleration for guiding an intense laser pulse [29], as well as for applications [30–34] such as high-quality radiation generation [35–40] and plasma channel diagnostics [41]. It requires several intense Gaussian laser pulses equally arranged along a circle and injected into the plasma channel simultaneously. A schematic of the method with initially three Gaussian pulses is shown in Figs. 1(a) and 1(b). Each of them undergoes a centroid oscillation since it experiences an asymmetric transverse focusing force periodically [35,36,38,42]. Once combined in the plasma, they are helically guided by the principle of optical refraction [43] and together form a specific ultraintense OVB, a modified Bessel-Gaussian beam (MBGB) [44]. Unlike a LGB which is a kind of Gaussian beam, a MBGB is a bounded Bessel beam [45] with the amplitude restricted by a Gaussian profile and modulated by a summation of modified Bessel functions. In plasma, the well-controlled OAM carried by the MBGB is encoded in the helical oscillation. The OVB is not only stable in a plasma but also survives in vacuum, and thus enables various applications.

\*b.lei@hi-jena.gsi.de

†bin.liu@gsi.de

‡S.Rykovanov@skoltech.ru

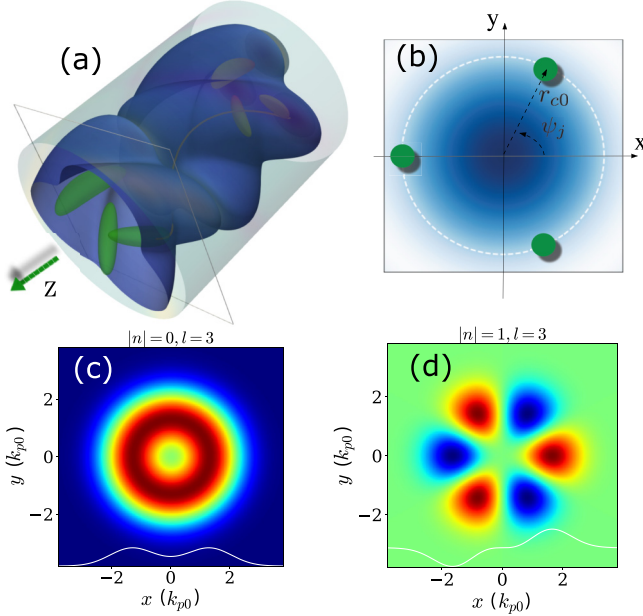


FIG. 1. (a) Schematic of PBB scheme in a parabolic plasma channel with three Gaussian pulses (green beamlets). Each pulse undergoes a centroid oscillation around the channel center along the  $z$  axis (green arrow) with a helical trajectory (orange line). A plasma wave is excited with a twisted structure (blue surface). Electrons can be trapped and accelerated to form the structured beam (yellow beamlets at the back). (b) Transverse slice at the position indicated by the gray frame in (a). One of the laser pulses (green spots) is indicated with its initial offset  $r_{c,0}$  and centroid tilt  $\psi_j$ . The transverse density gradient of the plasma channel is indicated by the blue-white color. (c), (d) Numerical result of the initial field structure of the first two vortex submodes of the MBGB,  $|n| = 0, 1$ . The white curves are the plots of the field along the  $x$  axis at  $y = 0$ .

At first we analyze the centroid harmonic oscillation of one of the Gaussian pulses, the quantities of which are denoted by the subscript  $j$ . If the initial injection of the laser pulse is specifically set to excite the transverse centroid oscillation with the amplitudes in each direction as  $r_{j,c0} = \sqrt{x_{j,x0}^2 + \theta_{j,x0}^2 Z_{j,R}^2} = \sqrt{y_{j,y0}^2 + \theta_{j,y0}^2 Z_{j,R}^2}$  and the transverse centroid tilt as  $\psi_{j,x0} = \psi_{j,y0} \pm \pi/2 = \psi_j$ , it has a stable helical centroid trajectory as  $\mathbf{r}_{j,c}(t) = (r_{j,c0}/2)\boldsymbol{\epsilon}_j \exp(i\Omega_{j,c}t) + \text{c.c.}$  over several Rayleigh lengths  $Z_{j,R}$  [46]. Here,  $\psi_{j,k0} = \arctan(k_{j,0}/\theta_{j,k0}Z_{j,R})$ , where  $k$  presents either the  $x$  or  $y$  direction, as shown in Fig. 1(b). This condition can be achieved by tuning the initial offset  $(x_{j,0}, y_{j,0})$  and angle  $(\theta_{j,x0}, \theta_{j,y0})$  separately in each direction. The centroid oscillation frequency is  $\Omega_{j,c} \simeq 1/Z_{j,R}$ . The complex vector  $\boldsymbol{\epsilon}_j = (1, \pm i)$  describes a left- or right-handed helix about the  $z$  axis and depends on the initial offset and angle. In this Letter, the case of the left helix  $\boldsymbol{\epsilon}_j = (1, i)$  is considered. As a result, the azimuthal dependence is introduced into the Gaussian pulse and the vector potential is modified to be decentered as  $\mathbf{a}_j(\mathbf{r}, \tau, \zeta) = \hat{\mathbf{x}} \cdot \tilde{\mathbf{a}}_j(\mathbf{r}, \tau, \zeta) g_j(\zeta) e^{iM_{j,p}\zeta}/2 + \text{c.c.}$ , where  $\tau = t$ ,  $\zeta = z - \tau$ .  $g_j(\zeta)$  and  $\tilde{\mathbf{a}}_j(\mathbf{r}, \tau, \zeta) = a_{j,0} \exp\{-[\mathbf{r} - \mathbf{r}_{j,c}(\tau, \zeta)]^2/w_{j,0}^2\}$  are the normalized spatial and temporal envelopes, respectively, with  $a_{j,0} = eA_{j,0}/m_e c^2$  the normalized laser strength,  $A_{j,0}$  the vector of the laser field,  $M_{j,p}$  the normalized laser frequency,

and  $w_{j,0}$  the matched laser spot size [43]. Note that throughout this Letter, the length is in units of the plasma wave number  $k_{p0} = \sqrt{4\pi n_0 e^2/(m_e c^2)}$ , where  $n_0$  is the initial plasma electron density along the channel axis,  $m_e$  the rest mass of the electron,  $c$  the speed of light in vacuum, and the time is in units of  $\omega_{p0} = k_{p0}c$ . The electric field is in units of the plasma wave breaking field along the channel axis  $E_{wb} = e/m_e c^2 k_{p0}$ . In the cylindrical coordinate  $(r, \phi, z)$ , the spatial envelope for the laser pulse is written as

$$\tilde{a}_j(r, \phi, \tau) = a_{0,j} e^{-\frac{r^2 + r_{j,c0}^2 - 2rr_{j,c0} \cos(\Omega_{j,c}\tau + \phi + \psi_j)}{w_{j,0}^2}}, \quad (1)$$

where the helical guiding imprints the transverse tilt  $\psi_j$  on the pulse front.

The superposition of all the injected pulses with the same frequency  $M_{j,p} = M_p$ , initial spot size  $w_{0,i} = w_0$ , and transverse offset  $r_{c0,j} = r_{c0}$ , but different  $\psi_j = 2\pi j/l$ , is written as

$$\begin{aligned} \tilde{a}(r, \phi, \tau) &= \sum_{j=1}^l \tilde{a}_j(r, \phi, \tau) \\ &= C_0 l e^{-\frac{r^2}{w_0^2}} \sum_{n=-\infty}^{+\infty} I_{nl} \left( \frac{2r_{c0}r}{w_0^2} \right) e^{inl(\Omega_c \tau + \phi + \psi_0)}, \end{aligned} \quad (2)$$

where  $l$  is chosen such that  $l < 2\pi r_{c0}/w_0$  to avoid significant beam overlap and the accompanying pulse-pulse interactions.  $C_0 = a_0 e^{-r_{c0}^2/w_0^2}$ , and  $I_n$  are the modified Bessel functions of the first kind.  $\psi_0$  represents the initial reference phase which can be arbitrarily set to zero. See Supplemental Material for the derivation of Eq. (2) [47]. The composed laser pulse in Eq. (2) describes a guided  $I_0$ -type MBGB with a summation of infinite discrete vortex submodes of index number  $nl$ . Each carries a well-defined OAM characterized by the Hilbert factor  $e^{inl\phi}$  except the mode  $n = 0$ . The field structures of the first two modes are shown in Figs. 1(c) and 1(d), where the intensity is dominated by the first mode  $n = 0$  and the vortex structure by the second mode  $|n| = 1$  depending on the number of subpulses. Therefore, the constituent of modes and then its topological structure can be flexibly tuned over the parameter  $l$ .

The fundamental property of the OAM initially carried by the MBGB can be understood by taking the ratio of  $z$  components of the total angular momentum density  $M_z = \text{Re}\{(\mathbf{r} \times [\mathbf{E} \times \mathbf{B}])_z\}$  to the linear momentum density  $S_z = \text{Re}\{\mathbf{E} \times \mathbf{B}\}_z$  of the field [48],

$$\frac{M_z}{S_z} = \frac{l}{M_p} \frac{l\Omega_c}{M_p} \Lambda_z, \quad (3)$$

where  $l/M_p$  represents the vortex nature,  $l\Omega_c/M_p$  shows that the OAM is encoded by the centroid oscillation of  $l$  subpulses, and the coupling coefficient  $\Lambda_z = (\sum_n n A_n e^{inl\xi} / \sum_n A_n e^{inl\xi})^2$  evaluates how the submodes contribute to the total OAM, with  $A_n = I_{nl} e^{-r^2/w_0^2}$ . The total OAM of the MBGB with the initial spot size of subpulses  $w_0$  is directly obtained by calculating the integral of  $M_z$ ,

$$L_z = \int M_z d^3r = 2\pi C_0^2 l^4 \Omega_c \sigma_l \sum_n n^2 A_n, \quad (4)$$

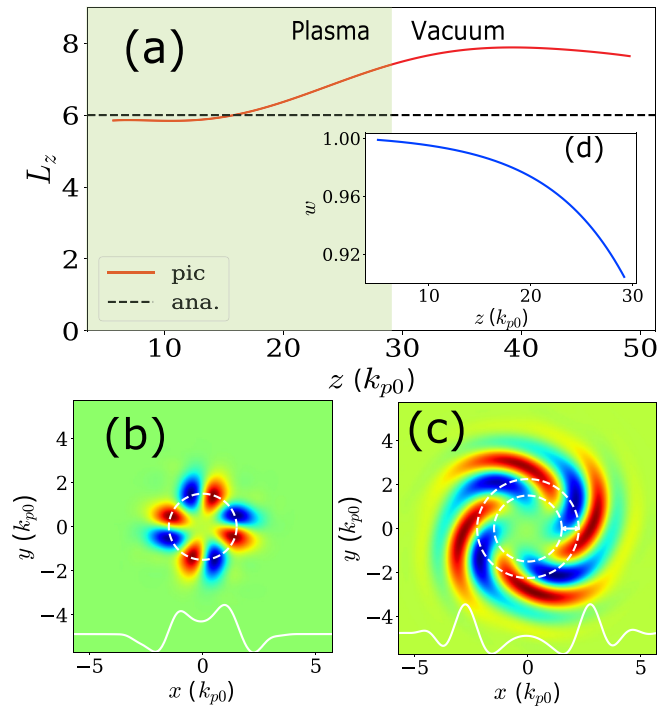


FIG. 2. 3D PIC results of MBGB with the following parameters:  $a_0 = 3$ ,  $n_0 = 1 \times 10^{18} \text{ cm}^{-3}$ ,  $w_0 = 1$ , and  $r_{c0} = 1.5$ . (a), (d) Evolution of total OAM  $L_z$  as transiting from the plasma into vacuum.  $L_z$  is in units of  $L_{z0} = k_{p0}^4 E_{wb}^2 / c$ . With the parameters used here,  $L_{z0} = 1.9 \times 10^{18} \hbar$ , where  $\hbar$  is the reduced Planck constant. The analytical result is obtained by using Eq. (4) with an initial  $w_0$ . The evolution of the spot size  $w$  of a single subpulse as a function of propagation distance is shown in the inserted figure, which is calculated by helically propagating one of the subpulses in the plasma with the same injection condition. (b), (c) Electric field of four pulses after propagating  $z = 27$  (or  $140 \mu\text{m}$ ) in a plasma channel and  $z = 38$  (or  $200 \mu\text{m}$ ) in vacuum after leaving the plasma. The small dashed circles in (b) and (c) indicate the initial center of the subpulses. The outer circle in (c) indicates the center in vacuum at this point  $z = 57$ . The radius is increased by  $0.57$  (or  $3 \mu\text{m}$ ).

where  $\sigma_l = \int_{-\infty}^{+\infty} g^2(\zeta') d\zeta'$ .  $\mathcal{A}_n = \int_0^{+\infty} r I_{nl}^2 e^{-2r^2/w_0^2} dr = \frac{\sqrt{\pi}}{4w_0^2} \left( \frac{2r_{c0}^2}{w_0^2} \right)^{nl} \frac{{}_1F_1(1/2+nl; 1+2nl; 2r_{c0}^2/w_0^2)}{\Gamma(1/2-nl)\Gamma(1+2nl)}$ , where  ${}_1F_1$  and  $\Gamma$  are the Kummer confluent hypergeometric and Euler gamma functions, respectively. It is easy to find from Eq. (4) that  $L_z$  increases with a transverse offset but decreases with a spot size of the laser subpulse. As a result,  $L_z$  evolves with the offset and spot size varying during propagation in the plasma channel. Furthermore, the mode with a larger  $l$  plays a more important role in forming  $L_z$ .

In order to confirm the theoretical analysis, full three-dimensional particle-in-cell (3D PIC) simulations have been performed with four spatial Gaussian laser pulses  $l = 4$  by using EPOCH [49] on the supercomputer JUWELS [50]. A guided MBGB is formed as expected. Due to the refractive guiding effect, it propagates stably in the plasma as seen in Fig. 2(b). The associated OAM during the propagation is shown in Fig. 2(a). This agrees with the theoretical prediction calculated from Eq. (4) with the initial parameters. Due to the plasma guiding effect, the OAM can be significantly higher

than that of LGBs in vacuum with a similar intensity, e.g., that in Ref. [25]. Furthermore, the OAM increases slowly with time. This can be interpreted as a result of self-focusing of the laser subpulses, as is seen in Fig. 2(d), which is mainly determined by the initial plasma configuration, and is adjustable. This also shows that the method proposed here does not require a strict matching condition on the stable guiding of laser subpulses, indicating that the method is robust. More details of the robustness will be discussed later. Once leaving the plasma channel, each subpulse becomes unguided and then the MBGB should be deconstructed. For the purpose of seeing this in the simulation, the plasma is cut off deliberately at  $z = 27$ . Surprisingly, the deconstruction process is very slow. The electric field is twisted gradually. A snapshot of the electric field after propagating in vacuum for three Rayleigh lengths is shown in Fig. 2(c) in which a vortex pattern is clearly seen.

One of the most attracting phenomena of ultraintense OVBS is the excitation of helical plasma waves in an underdense plasma, which is important for applications including off-axis ionization injection electron acceleration [17], positively charged particle acceleration [8,9], and axial magnetic field generation [11]. Most of them mainly depend on the spatial vortex structure of the beating intensity. The MBGB generated in our case has a well-controlled vortex structure due to the mixture of the submodes, especially the beating between the first two modes as

$$I = \tilde{a}\tilde{a}^* \simeq C_0^2 l^2 e^{-\frac{2r^2}{w_0^2}} (I_0^2 + 4I_1 I_0 \cos l\xi), \quad (5)$$

where  $\xi = \Omega_c \tau + \phi$ , and the high-frequency terms,  $|n| > 2$ , are of small amplitude and neglected. A snapshot of the intensity is shown in Fig. 3(a). It is clearly seen that the most intense part of the intensity is confined in the surrounding four lobes. In the following, we show that a guided MBGB is capable of accelerating particles and exciting an extremely strong magnetic field in the plasma.

The 3D PIC simulations have been performed by using EPOCH [49] on JUWELS [50] with a short section of uniform  $\text{N}^{5+}$  ions 2% of  $n_0$  mixed with fully ionized hydrogen in the beginning ( $0 \leq z \leq 38$ ) to control the location of the injection [51]. See Supplemental Material for the configuration of the simulations [47].

The generated wakefield shows an  $l$ -lobe structure which is inherited from the intensity structure of the MBGB. The lobe structure of the plasma wave on the  $xz$  plane is indicated by the dashed red ellipses as shown in Fig. 3(b). Electrons ionized from the  $K$  shell of  $\text{N}^{5+}$  can be trapped inside each lobe and combined to form a spatially vortex-structured electron beam as shown in Fig. 3(e) with a total OAM of about 0.04% of that initially carried by the MBGB. With an increase in time, this vortex electron beam is gradually squeezed to form a ring structure with a ring current of amplitude in the order of  $10^{12} \text{ A/m}^2$ . Such structured electron beams have been proposed for polarized radiation [52], or for improving the betatron radiation quality [15]. The capability of ionization injection and efficient acceleration may also be helpful for overcoming the depolarization issue in generating relativistic polarized electron beams if circularly polarized laser subpulses are used [14]. The on-channel-axis electric field with a very high acceleration gradient is shown in Fig. 3(c). It can



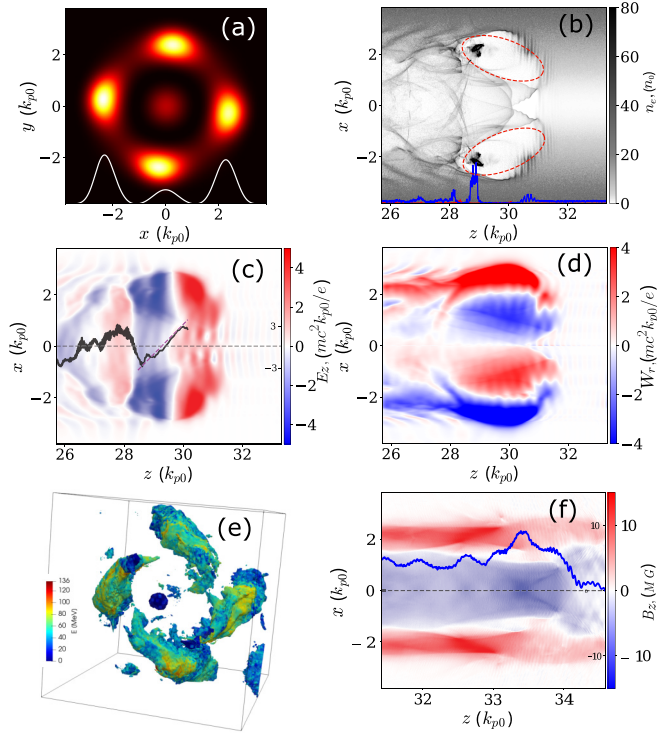


FIG. 3. Plasma wakefield at  $\tau = 32$  (or  $z' = 170 \mu\text{m}$ ). (a) Initial intensity structure of MBGB in the plasma. The field along the  $x$  axis at  $y = 0$  is plotted by a white curve on the bottom. (b) Longitudinal slice of the background plasma density distribution in the  $xz$  plane at  $y = 0$ . Red and blue curves present the plot along the  $z$  axis at  $x = 0$  and  $x = 1.5$ , respectively. The dashed red ellipses indicate the region of the lobe structure of the plasma wave. (c) Slice of longitudinal field  $E_z$ . The solid black curve shows the plot of  $E_z$  along the  $z$  axis at  $x = 0$  and the dashed magenta line shows the numerical approximation in the first bubble region. (d) Slice of transverse focusing field  $W_r$ . (e) Density distribution of a twisted electron beam at  $\tau = 72$  in 3D. (f) Slice of an axial magnetic field after the MBGB. The field along the  $z$  axis at  $x = 0$  (indicated by the dashed line) is plotted by the blue curve, with a maximum value close to 10 MG.

be numerically approximated as  $E_z \simeq l\zeta/2$  which is  $l$  times higher than that in a bubble excited by a single pulse [53] and can be used for accelerating positively charged particles. This is a special benefit from the transverse focusing field, as shown in Fig. 3(d), which is an important and interesting feature of OVB-driven wakes [8,9]. An extremely strong and sustainable axial magnetic field is generated due to the fluid vorticity of the plasma electrons [54]. It spans in a longitudinal range of tens of  $\mu\text{m}$  and a peak value of  $>10$  MG along the channel axis, and moves together with the MBGB as shown in Fig. 3(f).

The realization of the method proposed in this Letter requires multi-Gaussian laser pulses. This is the current trend in laser plasma research as various applications with a similar requirement have been proposed, for example, in plasma wakefield acceleration [55–57], strong-field QED [58,59], polarized electron sources [60], and others [61–63]. The experimental realization with four high-intensity laser pulses, as is used in our simulations, can be achieved by using a serrated

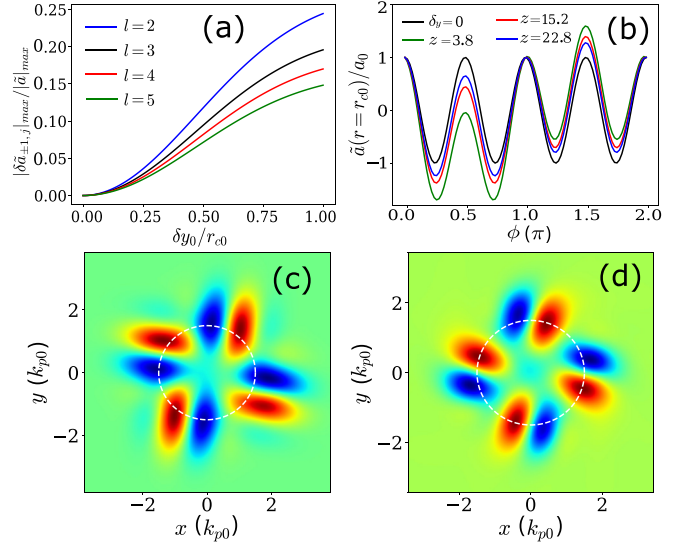


FIG. 4. (a) Ratio of MBGB field amplitude perturbation  $|\delta\tilde{a}_j|/|\tilde{a}|$  on the dominating vortex mode  $|n| = 1$  due to the inaccuracy on the laser injection offset  $\delta y_{j,0}$ , calculated at  $r = r_{c0}$  by Eq. (6). (b) Field amplitude in the azimuthal direction at different propagation times along the path  $r = r_{c0}$  indicated by the white dashed lines in (c) and (d). Black solid line: Analytical result with  $\delta y_{j,0} = 0$ . (c) and (d) Transverse MBGB field with initial  $\delta y_{j,0} = 0.25 r_{c0}$  at longitudinal positions  $z = 3.8$  and  $22.8$ , respectively.

aperture [64] before the main amplifier to separate the laser beam. This ensures energy efficiency and stable propagation. Then, a concave mirror controls the injection offset and the angle to the plasma channel. See Supplemental Material for the experimental setup [47]. Here, we show that the method can tolerate an acceptable inaccuracy of the initial injection condition of the laser pulses. Since an inaccuracy on the offset or angle has the same effect on helical guiding, it is identical to study either of them, for example, a variation for the  $j$ th laser subpulse in the  $y$  direction as  $y'_{j,0} = y_{j,0} + \delta y_{j,0}$ . The maximum perturbation for each mode at  $r = r_{c0}$  is given as

$$\delta\tilde{a}_{n,j} = C_0 e^{-\frac{r_{c0}^2}{w_0^2}} I_n \left( \frac{2r_{c0}^2}{w_0^2} \right) \times \left[ \beta_j \sum_{m=-\infty}^{+\infty} (-i)^m I_m \left( \frac{r_{c0} \delta y_{j,0}}{w_0^2} \right) - 1 \right], \quad (6)$$

where  $\beta_j = e^{(r_{c0} \delta y_{j,0} \sin \psi_j - 2\delta y_{j,0}^2)/2w_0^2}$ . See Supplemental Material for the derivation of Eq. (6) [47]. It is seen that the dominated  $m = 0$  mode is insensitive for an inaccuracy  $\delta y_{j,0}/r_{c0} < 0.25$  as shown in Fig. 4(a). It also shows that a MBGB constructed by more subpulses, i.e., larger  $l$ , is more robust. The MBGB also has the ability of self-reorganizing for small perturbation, as shown in Figs. 4(b)–4(d), where the imperfectly constructed MBGB is gradually corrected as it is being helically guided. This feature ensures that a distorted beam can propagate for several Rayleigh lengths in a plasma. It fails only when the initial inaccuracies are too large so that the helical guiding is destroyed.

In conclusion, the generation of a relativistic guided modified Bessel-Gaussian optical beam (MBGB) via the

plasma-based braiding (PBB) method has been demonstrated. This method of constructing ultraintense OVBs directly at focus allows for an acceptable inaccuracy of the initial setup conditions and thus is robust. It provides a promising alternative for producing relativistic OVBs in laboratories. Therefore, we believe this work will enhance the research interest in ultraintense OVBs and the related practical applications involving advanced optics, including the vortex-related strong-field light-matter interaction.

B.L. would like to acknowledge Jianxin Li for fruitful discussions. This work was supported by the Helmholtz Association (Young Investigator's Group VH-NG-1037). The authors gratefully acknowledge the computing time granted by the John von Neumann Institute for Computing (NIC) and provided on the supercomputer JUWELS at Jülich Supercomputing Centre (JSC). The authors acknowledge the usage of the Skoltech CDISE HPC cluster Zhores [65] for obtaining part of the results presented in this Letter.

- 
- [1] J. F. Nye, M. V. Berry, and F. C. Frank, *Proc. R. Soc. London, Ser. A* **336**, 165 (1974).
- [2] Y. Shen, X. Wang, Z. Xie, C. Min, X. Fu, Q. Liu, M. Gong, and X. Yuan, *Light: Sci. Appl.* **8**, 90 (2019).
- [3] L. Zhang, B. Shen, X. Zhang, S. Huang, Y. Shi, C. Liu, W. Wang, J. Xu, Z. Pei, and Z. Xu, *Phys. Rev. Lett.* **117**, 113904 (2016).
- [4] L. B. Ju, T. W. Huang, K. D. Xiao, G. Z. Wu, S. L. Yang, R. Li, Y. C. Yang, T. Y. Long, H. Zhang, S. Z. Wu, B. Qiao, S. C. Ruan, and C. T. Zhou, *Phys. Rev. E* **94**, 033202 (2016).
- [5] W. Wang, B. Shen, X. Zhang, L. Zhang, Y. Shi, and Z. Xu, *Sci. Rep.* **5**, 8274 (2015).
- [6] A. M. Summers, X. Yu, X. Wang, M. Raoul, J. Nelson, D. Todd, S. Zigo, S. Lei, and C. A. Trallero-Herrero, *Opt. Express* **25**, 1646 (2017).
- [7] J. Flick, N. Rivera, and P. Narang, *Nanophotonics* **7**, 1479 (2018).
- [8] S. Gessner, E. Adli, J. M. Allen, W. An, C. I. Clarke, C. E. Clayton, S. Corde, J. P. Delahaye, J. Frederico, S. Z. Green *et al.*, *Nat. Comm.* **7**, 11785 (2016).
- [9] J. Vieira and J. T. Mendonça, *Phys. Rev. Lett.* **112**, 215001 (2014).
- [10] S. Kumar, A. Parola, P. Di Trapani, and O. Jedrkiewicz, *Appl. Phys. B* **123**, 1432 (2017).
- [11] Y. Shi, J. Vieira, R. M. G. M. Trines, R. Bingham, B. F. Shen, and R. J. Kingham, *Phys. Rev. Lett.* **121**, 145002 (2018).
- [12] R. Nuter, P. Korneev, I. Thiele, and V. Tikhonchuk, *Phys. Rev. E* **98**, 033211 (2018).
- [13] J. Handali, P. Shakya, and B. Barwick, *Opt. Express* **23**, 5236 (2015).
- [14] Y. Wu, L. Ji, X. Geng, Q. Yu, N. Wang, B. Feng, Z. Guo, W. Wang, C. Qin, X. Yan, L. Zhang, J. Thomas, A. Hützen, M. Büscher, T. P. Rakitzis, A. Pukhov, B. Shen, and R. Li, *New J. Phys.* **21**, 073052 (2019).
- [15] J. Luís Martins, J. Vieira, J. Ferri, and T. Fülöp, *Sci. Rep.* **9**, 9840 (2019).
- [16] X. Zhang, B. Shen, Y. Shi, L. Zhang, L. Ji, X. Wang, Z. Xu, and T. Tajima, *New J. Phys.* **18**, 083046 (2016).
- [17] J. Vieira, J. T. Mendonça, and F. Quéré, *Phys. Rev. Lett.* **121**, 054801 (2018).
- [18] W. P. Putnam, D. N. Schimpf, G. Abram, and F. X. Kärtner, *Opt. Express* **20**, 24429 (2012).
- [19] L. Lin, P. Wang, and J. Liu, *Proc. SPIE* **10811**, 108111B (2018).
- [20] L. Rego, K. M. Dorney, N. J. Brooks, Q. L. Nguyen, C.-T. Liao, J. San Román, D. E. Couch, A. Liu, E. Pisanty, M. Lewenstein, L. Plaja, H. C. Kapteyn, M. M. Murnane, and C. Hernández-García, *Science* **364**, eaaw9486 (2019).
- [21] T. Yu, H. Xia, W. Xie, G. Xiao, and H. Li, *Results Phys.* **16**, 102872 (2020).
- [22] A. Longman, C. Salgado, G. Zeraoui, J. I. Apiñaniz, J. A. Pérez-Hernández, M. K. Eltahlawy, L. Volpe, and R. Fedosejevs, *Opt. Lett.* **45**, 2187 (2020).
- [23] A. Leblanc, A. Denoeud, L. Chopineau, G. Mennerat, P. Martin, and F. Quéré, *Nat. Phys.* **13**, 440 (2017).
- [24] J. Vieira, R. M. G. M. Trines, E. P. Alves, R. A. Fonseca, J. T. Mendonça, R. Bingham, P. Norreys, and L. O. Silva, *Nat. Commun.* **7**, 10371 (2016).
- [25] Y. Shi, B. Shen, L. Zhang, X. Zhang, W. Wang, and Z. Xu, *Phys. Rev. Lett.* **112**, 235001 (2014).
- [26] C. Brabetz, S. Busold, T. Cowan, O. Deppert, D. Jahn, O. Kester, M. Roth, D. Schumacher, and V. Bagnoud, *Phys. Plasmas* **22**, 013105 (2015).
- [27] A. Denoeud, L. Chopineau, A. Leblanc, and F. Quéré, *Phys. Rev. Lett.* **118**, 033902 (2017).
- [28] W. P. Wang, C. Jiang, H. Dong, X. M. Lu, J. F. Li, R. J. Xu, Y. J. Sun, L. H. Yu, Z. Guo, X. Y. Liang, Y. X. Leng, R. X. Li, and Z. Z. Xu, *Phys. Rev. Lett.* **125**, 034801 (2020).
- [29] C. G. Durfee and H. M. Milchberg, *Phys. Rev. Lett.* **71**, 2409 (1993).
- [30] C. G. R. Geddes, C. Toth, J. van Tilborg, E. Esarey, C. B. Schroeder, D. Bruhwiler, C. Nieter, J. Cary, and W. P. Leemans, *Nature (London)* **431**, 538 (2004).
- [31] J. Thomas, I. Y. Kostyukov, J. Pronold, A. Golovanov, and A. Pukhov, *Phys. Plasmas* **23**, 053108 (2016).
- [32] J. Luo, M. Chen, W. Y. Wu, S. M. Weng, Z. M. Sheng, C. B. Schroeder, D. A. Jaroszynski, E. Esarey, W. P. Leemans, W. B. Mori, and J. Zhang, *Phys. Rev. Lett.* **120**, 154801 (2018).
- [33] B. Lei, T. Teter, J. W. Wang, V. Y. Kharin, C. B. Schroeder, M. Zepf, and S. G. Rykovanov, *Phys. Rev. Accel. Beams* **22**, 071302 (2019).
- [34] A. J. Gonsalves, K. Nakamura, J. Daniels, C. Benedetti, C. Pieronek, T. C. H. de Raadt, S. Steinke, J. H. Bin, S. S. Bulanov, J. van Tilborg, C. G. R. Geddes, C. B. Schroeder, C. Toth, E. Esarey, K. Swanson, L. Fan-Chiang, G. Bagdasarov, N. Bobrova, V. Gasilov, G. Korn, P. Satorov, and W. P. Leemans, *Phys. Rev. Lett.* **122**, 084801 (2019).
- [35] S. G. Rykovanov, C. B. Schroeder, E. Esarey, C. G. R. Geddes, and W. P. Leemans, *Phys. Rev. Lett.* **114**, 145003 (2015).
- [36] M. Chen, J. Luo, F.-Y. Li, F. Liu, Z.-M. Sheng, and J. Zhang, *Light: Sci. Appl.* **5**, e16015 (2016).
- [37] J. P. Palastro, D. Kaganovich, B. Hafizi, Y.-H. Chen, L. A. Johnson, J. R. Peñano, M. H. Helle, and A. A. Mamonau, *Phys. Plasmas* **24**, 033119 (2017).

- [38] B. Lei, J. Wang, V. Kharin, M. Zepf, and S. Rykovanov, *Phys. Rev. Lett.* **120**, 134801 (2018).
- [39] G. Zhang, M. Chen, X. Yang, F. Liu, S. Weng, Y. Ma, D. Zou, T. Yu, F. Shao, and Z. Sheng, *Opt. Express* **28**, 29927 (2020).
- [40] Z. G. Deng, Z. M. Zhang, B. Zhang, S. K. He, J. Teng, W. Hong, K. G. Dong, Y. C. Wu, B. Zhu, and Y. Q. Gu, *Phys. Rev. E* **95**, 023206 (2017).
- [41] A. J. Gonsalves, K. Nakamura, C. Lin, J. Osterhoff, S. Shiraishi, C. B. Schroeder, C. G. R. Geddes, C. Tóth, E. Esarey, and W. P. Leemans, in *14th Advanced Accelerator Concepts Workshop*, edited by S. H. Gold and G. S. Nusinovich, AIP Conf. Proc. (AIP, Melville, NY, 2010), Vol. 1299, p. 150.
- [42] L. Ceurvorst, N. Ratan, M. C. Levy, M. F. Kasim, J. Sadler, R. H. H. Scott, R. M. G. M. Trines, T. W. Huang, M. Skramic, M. Vranic, L. O. Silva, and P. A. Norreys, *New J. Phys.* **18**, 053023 (2016).
- [43] E. Esarey, C. B. Schroeder, and W. P. Leemans, *Rev. Mod. Phys.* **81**, 1229 (2009).
- [44] S. R. Seshadri, *J. Opt. Soc. Am. A* **24**, 2837 (2007).
- [45] F. Gori, G. Guattari, and C. Padovani, *Opt. Commun.* **64**, 491 (1987).
- [46] S. G. Rykovanov, J. W. Wang, V. Y. Kharin, B. Lei, C. B. Schroeder, C. G. R. Geddes, E. Esarey, and W. P. Leemans, *Phys. Rev. Accel. Beams* **19**, 090703 (2016).
- [47] See Supplemental Material at <http://link.aps.org/supplemental/10.1103/PhysRevA.104.L021501> for additional information including: (1) derivation of super pulse construction and error tolerance estimation due to laser injection inaccuracy; (2) Configuration of PIC simulations; (3) feasible setup of laser pulses injection in current experimental conditions.
- [48] L. Allen, M. W. Beijersbergen, R. J. C. Spreeuw, and J. P. Woerdman, *Phys. Rev. A* **45**, 8185 (1992).
- [49] T. D. Arber, K. Bennett, C. S. Brady, A. Lawrence-Douglas, M. G. Ramsay, N. J. Sircombe, P. Gillies, R. G. Evans, H. Schmitz, A. R. Bell, and C. P. Ridgers, *Plasma Phys. Controlled Fusion* **57**, 113001 (2015).
- [50] Jülich Supercomputing Centre, *J. large-scale res. facilities* **5**, A135 (2019).
- [51] A. Pak, K. A. Marsh, S. F. Martins, W. Lu, W. B. Mori, and C. Joshi, *Phys. Rev. Lett.* **104**, 025003 (2010).
- [52] I. P. Ivanov and D. V. Karlovets, *Phys. Rev. A* **88**, 043840 (2013).
- [53] W. Lu, C. Huang, M. Zhou, W. B. Mori, and T. Katsouleas, *Phys. Rev. Lett.* **96**, 165002 (2006).
- [54] B. Talin, V. P. Kaftandjian, and L. Klein, *Phys. Rev. A* **11**, 648 (1975).
- [55] J. Faure, C. Rechatin, A. Norlin, A. Lifschitz, Y. Glinec, and V. Malka, *Nature (London)* **444**, 737 (2006).
- [56] M. Zeng, M. Chen, L. L. Yu, W. B. Mori, Z. M. Sheng, B. Hidding, D. A. Jaroszynski, and J. Zhang, *Phys. Rev. Lett.* **114**, 084801 (2015).
- [57] M. Wen, M. Tamburini, and C. H. Keitel, *Phys. Rev. Lett.* **122**, 214801 (2019).
- [58] C. Bamber, S. J. Boege, T. Koffas, T. Kotseroglou, A. C. Melissinos, D. D. Meyerhofer, D. A. Reis, W. Ragg, C. Bula, K. T. McDonald, E. J. Prebys, D. L. Burke, R. C. Field, G. Horton-Smith, J. E. Spencer, D. Walz, S. C. Berridge, W. M. Bugg, K. Shmakov, and A. W. Weidemann, *Phys. Rev. D* **60**, 092004 (1999).
- [59] I. C. E. Turcu, S. Balascuta, F. Negoita, D. Jaroszynski, and P. McKenna, in *Exotic Nuclei and Nuclear/Particle Astrophysics (V). From Nuclei to Stars: Carpathian Summer School of Physics 2014*, edited by L. Trache, D. Chesneanu, and C. A. Ur, AIP Conf. Proc. (AIP, Melville, NY, 2015), Vol. 1645, p. 416.
- [60] Z. Nie, F. Li, F. Morales, S. Patchkovskii, O. Smirnova, W. An, N. Nambu, D. Matteo, K. A. Marsh, F. Tsung, W. B. Mori, and C. Joshi, *Phys. Rev. Lett.* **126**, 054801 (2021).
- [61] T. Toncian, M. Borghesi, J. Fuchs, E. d'Humières, P. Antici, P. Audebert, E. Brambrink, C. A. Cecchetti, A. Pipahl, L. Romagnani, and O. Willi, *Science* **312**, 410 (2006).
- [62] S. M. Pfoth, O. Jäckel, J. Polz, S. Steinke, H.-P. Schlenvoigt, J. Heymann, A. P. L. Robinson, and M. C. Kaluza, *New J. Phys.* **12**, 103009 (2010).
- [63] J. M. Cole, K. T. Behm, E. Gerstmayr, T. G. Blackburn, J. C. Wood, C. D. Baird, M. J. Duff, C. Harvey, A. Ilderton, A. S. Joglekar, K. Krushelnick, S. Kuschel, M. Marklund, P. McKenna, C. D. Murphy, K. Poder, C. P. Ridgers, G. M. Samarin, G. Sarri, D. R. Symes, A. G. R. Thomas, J. Warwick, M. Zepf, Z. Najmudin, and S. P. D. Mangles, *Phys. Rev. X* **8**, 011020 (2018).
- [64] J. M. Auerbach and V. P. Karpenko, *Appl. Opt.* **33**, 3179 (1994).
- [65] I. Zacharov, R. Arslanov, M. Gunin, D. Stefonishin, A. Bykov, S. Pavlov, O. Panarin, A. Maliutin, S. Rykovanov, and M. Fedorov, *Open Eng.* **9**, 512 (2019).